

# Effect of Powder Characteristics on Fatigue Performance of Additively Manufactured 17-4 PH Stainless Steel

Arun Poudel, Arash Soltani-Tehrani, Shuai Shao, Nima Shamsaei\*

National Center for Additive Manufacturing Excellence (NCAME), Auburn University, Auburn,  
AL 36849, USA

Department of Mechanical Engineering, Auburn University, Auburn, AL 36849, USA

\* Corresponding author: [shamsaei@auburn.edu](mailto:shamsaei@auburn.edu)

## Abstract

The characteristics of powder feedstock used during laser powder bed fusion (L-PBF) influence the mechanical performance of the fabricated parts. The flowability, spreadability, and internal porosity of the powder can affect the porosity formation and thus, impact the fatigue performances. Two batches of 17-4 precipitation hardening stainless steel powders supplied by two different vendors were used to fabricate the L-PBF specimens and investigate the effect of powder characteristics on porosity and fatigue behavior. The powder batch with a wider particle size distribution, higher compressibility, higher cohesion between powder particles, and internal porosity resulted in a higher defect content in the fabricated specimens. Higher defect content led to inferior fatigue resistance along with more scatter in the fatigue lives. Fractography revealed the fatigue crack initiation from spherical pores as well as the lack of fusions in both batches.

**Keywords:** Additive manufacturing, Powder characteristics, Particle size distribution, Volumetric defects, Fatigue performance

## Introduction

Different additive manufacturing (AM) technologies such as laser powder bed fusion (L-PBF), laser powder directed energy deposition (LP-DED), electron beam directed energy deposition (EB-DED), etc., use metallic powder as feedstock during the fabrication process [1–5]. The physical characteristics of the feedstock powder such as particle size distribution, sphericity, internal porosity, etc., have been observed to influence the powder behavior during the AM processes [6]. Any influence in the powder behavior such as its flowability, spreadability, packing state, etc., can influence the porosity formation in the fabricated parts and thus, impact the mechanical properties [7–13]. Few studies have attempted to investigate the effect of powder characteristics on mechanical performances, especially fatigue performances [7–14].

One of the major characteristics influencing the powder's rheological behavior, and therefore the build quality, is the particle size distribution (PSD). It signifies the relative amount of different-sized powder particles in any specific batch. An AlSi7Mg powder with narrower PSD was observed to have lower cohesion between powder particles leading to better flowability and thus, higher density L-PBF parts [15]. On the other hand, iron powder with a wider PSD was observed to fabricate lower-density L-PBF parts [16]. The smaller iron powder particles were observed to agglomerate, resulting in a poor packing state during the L-PBF fabrication process. In addition, the powder batches with narrower PSD have been observed to possess a better packing

state resulting in lower compressibility [11,17]. In a powder recycling study of Ti-6Al-4V material, the recycled powder batch with narrower PSD was observed to have better flowability, resulting in fewer and smaller pores, and thus, better fatigue performance [11].

Rheological properties of the powder are also influenced by the particle's surface features such as satellites and the sphericity of the powder particles. The presence of satellites has been observed to increase the friction between the powder particles, impeding the flow of Ti-6Al-4V and nickel-based alloy powder [18]. It resulted in the parts with a lower density as well as lower ductility. In addition, the same study reported higher flowability of the powder with higher sphericity [18].

Although a few studies have been done to understand the effect of powder characteristics on mechanical performance, only limited research is available correlating its effect on the fatigue behavior of AM materials. Furthermore, America Makes and the American National Standards Institute (ANSI) have considered “*flowability*”, “*spreadability*”, “*particle size and particle size distribution*”, “*particle morphology*”, “*hollow particles and hollow particles with entrapped gas*”, and “*metal powder specifications*” as some of the major technical gaps (PM1, 4, 6, and 7) in the additive manufacturing standardization collaborative (AMSC) roadmap [19]. Hence, this study compared two different batches of 17-4 precipitation hardening (PH) stainless steel (SS) metallic powders obtained from different vendors and correlated the effect of powder characteristics on porosity formation as well as fatigue performance of L-PBF parts. The 17-4 PH SS alloy was selected due to its variety of applications in aerospace, oil refinery, and biomedical industries [20,21].

### **Material and Methods**

17-4 PH SS argon-atomized powders supplied by Carpenter Technology (i.e., Batch 1) and EOS (i.e., Batch 2) were utilized to fabricate cylindrical bars in EOS M290, an L-PBF AM machine. Bars were fabricated in a vertical orientation using recommended process parameters. The recommended process parameters for 17-4 PH SS include 220 W laser power, 756 mm/s laser speed, 100  $\mu\text{m}$  hatch distance, 40  $\mu\text{m}$  layer thickness, and 67° inter-layer rotation angle. The chemical compositions of both powder batches as reported by the powder's manufacturer are listed in **Table 1**. After fabrication, the bars were heat treated to CA-H1025 schedule as seen in **Fig. 1(a)** (i.e., solution annealing at 1050 °C for ½ hour followed by air cooling and aging at 552 °C for 4 hours followed by air cooling) [22]. The heat-treated bars were machined according to ASTM E466 [23] to final geometry shown in **Fig. 1(b)** and selected randomly from the build plate for fatigue testing. Fully-reversed force-controlled fatigue tests were performed at 500 MPa, 600 MPa, and 800 MPa stress levels using an MTS servo-hydraulic load frame.

After fatigue failure, fractography was performed to investigate the crack initiating defects using Zeiss Crossbeam 550 scanning electron microscope (SEM). Rheological properties of powders were investigated using Freeman Technology (FT4) powder rheometer according to ASTM D7891 [24], PSD using Anton Paar PSA 1190 based on laser diffraction technology [25], particle surface morphology using SEM, and internal porosity using Zeiss Xradia 620 Versa X-ray computed tomography (XCT) machine. The XCT scans were post-processed using ImageJ and Dragonfly Pro software [26,27]. In addition, the porosity in the fabricated specimens was investigated using Keyence VHX-6000 digital optical microscope. The porosity was investigated

in 4 different cross-sections (i.e., perpendicular to the building direction) throughout the gage-section of the specimens.

**Table 1** Chemical compositions of the 17-4 PH SS powders reported by the powder manufacturers.

Element (Wt. %)	Batch 1	Batch 2
C	0.010	0.010
Cr	16.300	16.670
Ni	4.180	4.270
Cu	4.100	3.680
Mn	0.220	0.050
Si	0.400	0.020
Nb	0.250	0.310
Mo	0.020	0.080
N	0.040	0.100
O	0.050	0.030
P	0.012	0.010
S	0.004	0.004
Fe	Bal.	Bal.

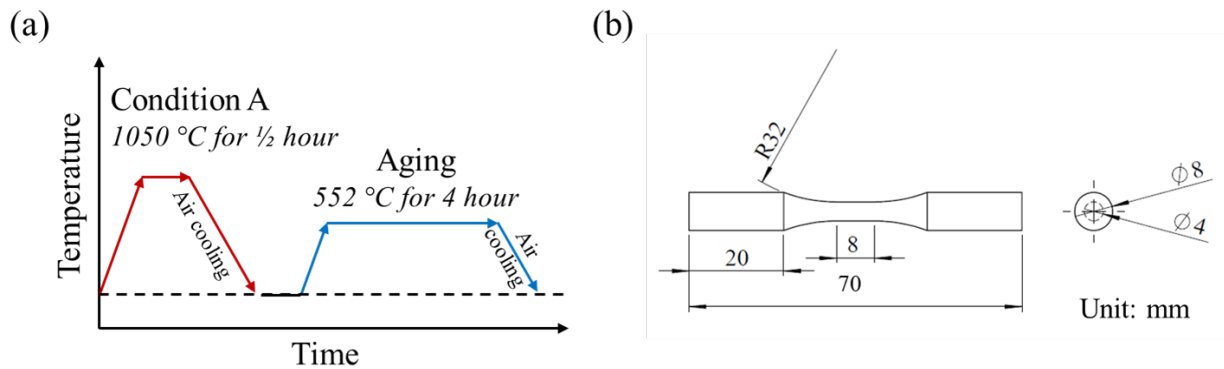


**Fig. 1** (a) CA-H1025 heat treatment schedule applied to 17-4 PH SS specimens. (b) The geometry of machined force-controlled fatigue specimens in accordance with ASTM E466 [23]. All dimensions are in mm.

## Results and Discussion

### Powder Characteristics

Various characteristics of the feedstock powder such as its shape, size distribution, internal porosities, etc. influencing the flowability, spreadability, packing state, agglomerate formation, etc. were investigated. The surface morphology of the powder particles representative of the considered powder batches was examined and shown in **Fig. 2**. In general, the average particle size of Batch 2 was higher as compared to Batch 1. Anomalies such as satellites were observed in both batches; however, it seemed to be higher for Batch 1 (see **Fig. 2(b & d)**). The presence of these satellites can increase interparticle friction and result in lower flowability and spreadability [28,29]. **Fig. 2(b)** shows the presence of open pores in Batch 1 powder. Regarding sphericity, it

seemed to be higher in Batch 2 as compared to Batch 1 (see **Figs. 2(b & d)**); however, a thorough analysis needed to be performed to support the statement. Higher sphericity has been observed to increase the spreadability of the powder particles [18].

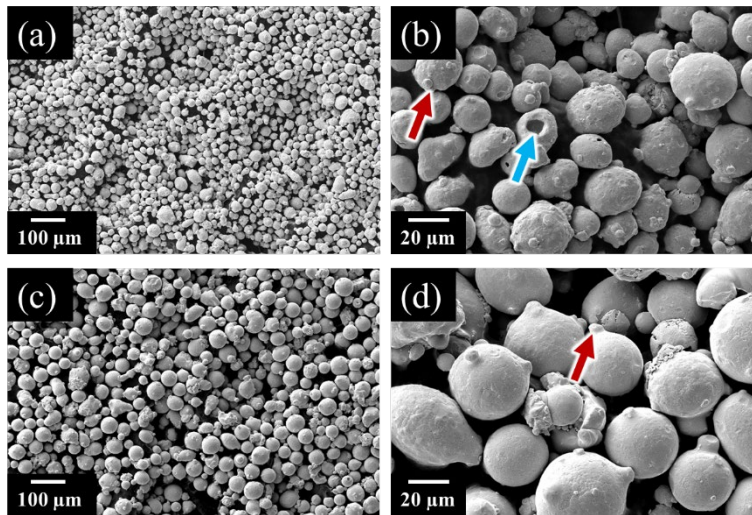


**Fig. 2** Particle morphology of (a & b) Batch 1 and (c & d) Batch 2 powder. Red and blue arrows point to satellites and open pores in the powder particles, respectively.

The PSD of each powder batch was investigated three times and their average is shown in **Fig. 3**. The average particle size in Batch 2 was observed to be larger than in Batch 1. In addition, Batch 1 contained a larger number of smaller particles as compared to Batch 2. The smaller powder particles tend to adhere with each other and also with larger particles, and form agglomerates [9,16]. Such agglomerates can result in lower flowability as well as a poor packing state of the powder due to the presence of air/void between them. **Fig. 3(c)** presents the  $D_{10}$ ,  $D_{50}$ , and  $D_{90}$  measures of both powder batches, where  $D_x$  signifies that  $x\%$  of the powder particles is below its value. The  $D_{10}$ ,  $D_{50}$ , and  $D_{90}$  for Batch 2 were 40%, 43%, and 38% higher as compared to Batch 1. As seen in the plot, the  $D_{10}$ s of Batch 1 and Batch 2 are smaller than  $21.7 \mu\text{m}$  and  $30.4 \mu\text{m}$ , respectively. This further validates the statement that Batch 1 is more prone to the formation of agglomerates as compared to Batch 2. From the previous study, the compressibility—which signifies the amount of air in between the powder particles—of Batch 1 was 67% higher than Batch 2 [14]. In addition, a good correlation was observed between the shear stress required for the powder batch to flow at different applied normal stresses. Batch 1 required higher shear stress to flow as compared to Batch 2 suggesting higher friction or resistance in between the Batch 1 powder particles. This behavior was attributed to the higher cohesion (i.e., two times) in between Batch 1 powder particles as compared to Batch 2 [14].

The span (i.e.,  $\text{span} = (D_{90}-D_{10})/D_{50}$ ) was calculated to be 0.8 and 0.76 for Batch 1 and Batch 2, respectively [29]. The lower span of Batch 2 indicates a narrower PSD and a more uniform particle size. Typically, fine particles attaching to larger particles have been observed to degrade powder's flowability and spreadability characteristics. Hence, it can be expected that the Batch 2 powder particles flow more smoothly and uniformly across the build plate as compared to Batch 1.

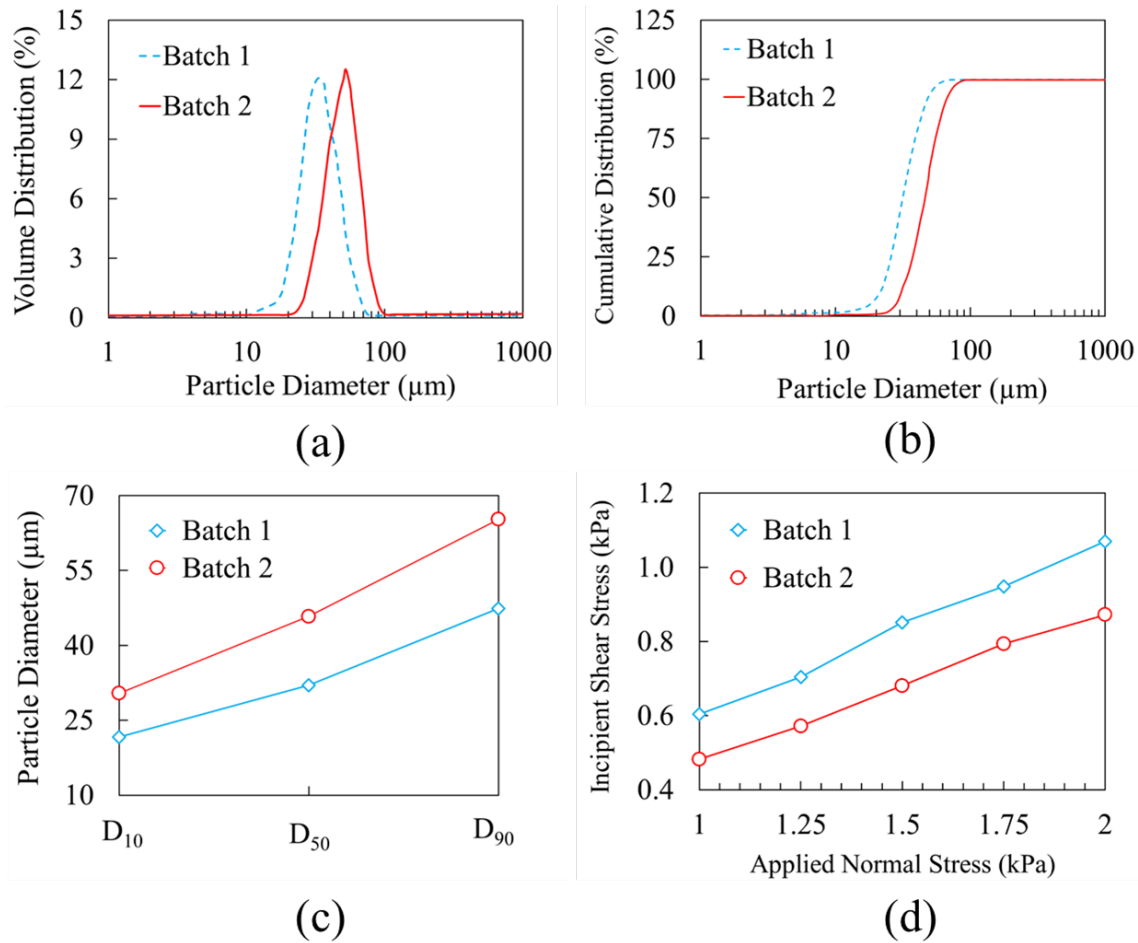


**Fig. 3** Comparison of PSD between powder batches: (a) Volumetric probabilistic density distribution, (b) cumulative density distribution, and (c)  $D_{10}$ ,  $D_{50}$ , and  $D_{90}$  measurements. (d) The comparison of the shear stress required for the powders to flow at different stress levels.

### **Porosity in Powder Particles and Fabricated Specimens**

The XCT findings of both powder batches are illustrated in **Fig. 4**. The voxel size of  $0.73 \mu\text{m}$  was used during the XCT scans of  $0.3055 \text{ mm}^3$  volume. In general, Batch 1 contains smaller but more internal pores as compared to Batch 2. A few large-size internal pores were evident in Batch 2 as seen in **Figs. 4(d-f)**. The largest pores inside the powder particles in both batches were in the range of  $30 \mu\text{m}$  to  $33 \mu\text{m}$ . During fabrication, these entrapped pores inside the powder particles may escape from the melt-pool; however, if the Marangoni force—which can push the gas bubbles downward—is higher than the buoyancy force, these particles get trapped in the substrate during the solidification process [30]. The presence of a large number of internal pores in Batch 1 powder particles as well as its poorer packing state made it susceptible to the formation of a higher degree of volumetric defects in the fabricated parts [31–33]. The statistics of the intra-particle pores is presented in **Fig. 5(a)**. As shown, the pore count in Batch 1 powder was significantly higher than in Batch 2 for most size ranges. During the analysis, defects with sizes smaller than  $10 \mu\text{m}$  were discarded.

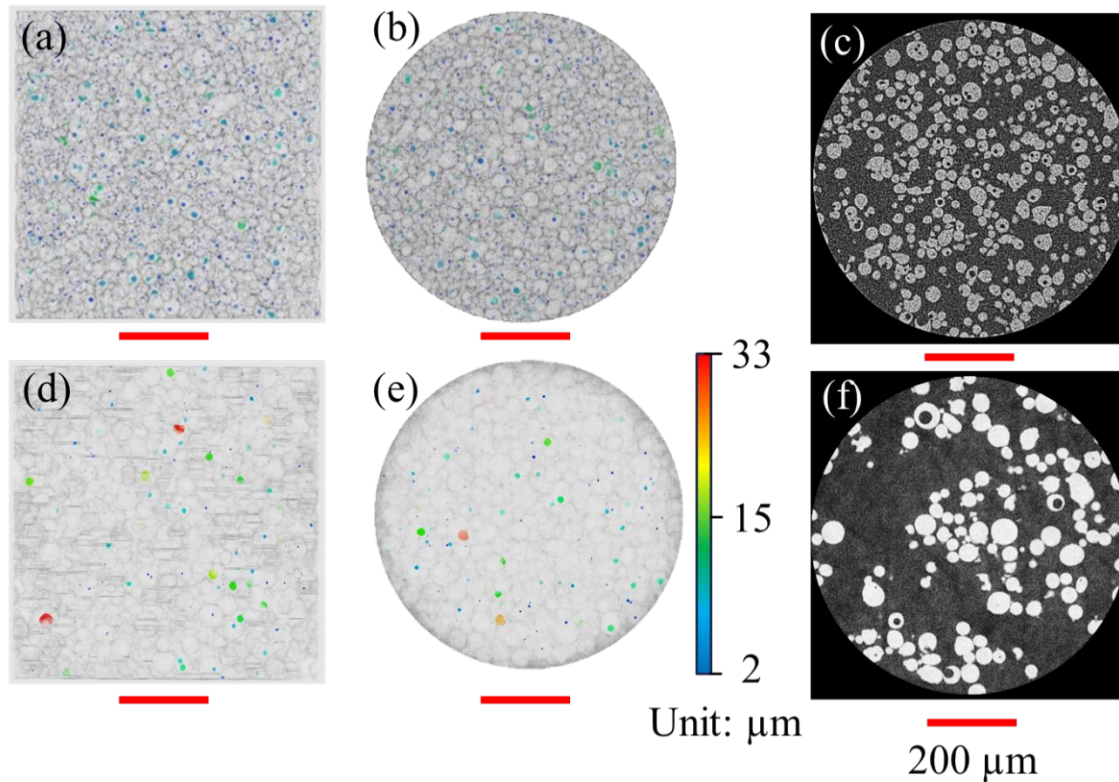


**Fig. 4** Internal porosities observed in (a & b) Batch 1 and (d & e) Batch 2 powder particles. The color scale signifies the equivalent diameter of internal pores in the  $\mu\text{m}$  scale. In addition, one volumetric scan slice from (c) Batch 1 and (f) Batch 2 is presented.

After fabrication, porosity analysis of specimens was performed using digital optical microscopy to investigate the influence of powder characteristics on defect content (see **Fig. 5(b)**). Parts fabricated using Batch 1 resulted in more volumetric defects for all size ranges. The size range of the defects observed in both powder particles and specimens was similar. In addition, the standard deviation observed during porosity analysis between 4 different layers was found to be higher for Batch 1 specimens. The observation made in **Fig. 5(b)** agrees with the earlier findings regarding flowability, packing state, as well as internal porosity in the powder particles. The presence of agglomerates and poor spreadability across the build plate for Batch 1 might have resulted in a non-uniform powder layer during the fabrication process. In addition, the presence of a higher degree of intra-particle porosity in Batch 1 (see **Fig. 4**) exacerbated the process and resulted in a higher porosity.

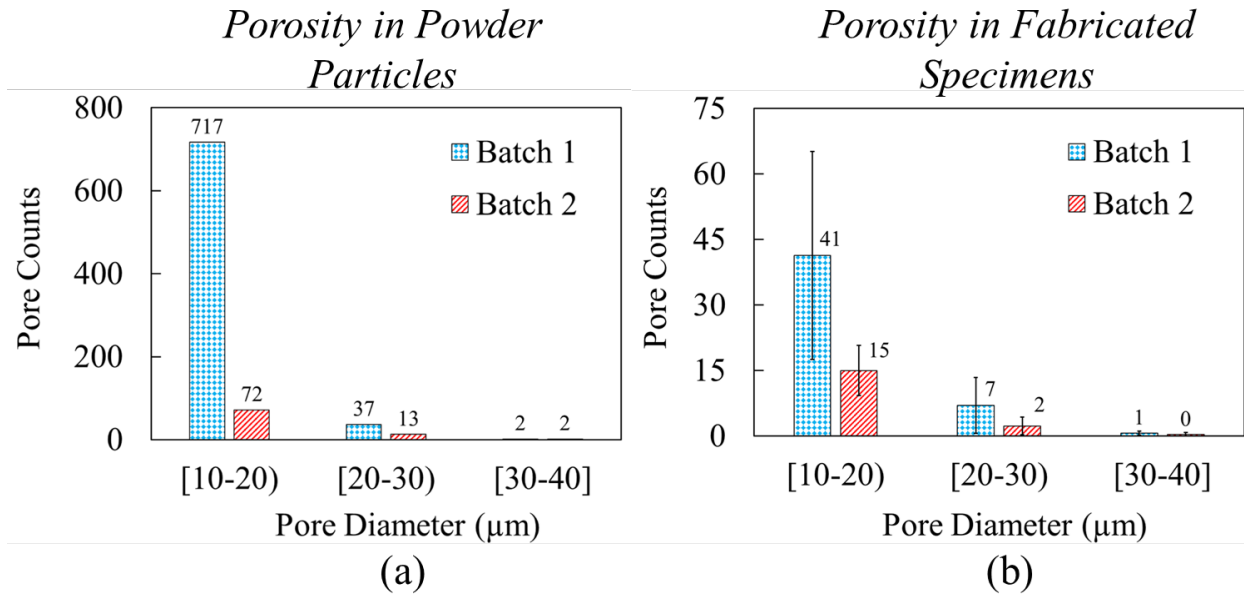


**Fig. 5** Size distributions of defects observed in (a) particles of the two powder batches via XCT and (b) fabricated specimens via digital optical microscopy.

### **Fatigue Performance**

The stress-life fatigue behavior of specimens fabricated using both powder batches is shown in **Fig. 6**. The fatigue behavior of Batch 1 specimens was adapted from Soltani-Tehrani et al. [9]. The fatigue resistance of both powder batches was comparable at low cycle fatigue (LCF) regime. It was attributed to the similar microstructure in both materials after being subjected to the same, CA-H1025 heat treatment schedule. However, the difference was more prominent in mid-cycle fatigue (MCF) and high cycle fatigue (HCF) regimes. The fatigue lives observed for Batch 2 specimens were higher in MCF and HCF regimes as compared to Batch 1. Furthermore, one Batch 2 specimen tested at 500 MPa was observed to be run out (i.e., exceeded five million cycles). Since the fatigue resistance of the material is more sensitive to the volumetric defects in HCF, the scatter was also observed to be higher at HCF for both powder batches. The higher level of porosity observed in Batch 1 specimens as compared to Batch 2 (see **Fig. 5(b)**) agrees with the fatigue performances observed in **Fig. 6**.

Fractography was performed to examine the crack initiating defects in both batches of specimens. Since the fatigue specimens were machined and polished to a mirror finish, the effect of surface roughness was eradicated and the cracks were observed to have initiated from the volumetric defects. In both batches, cracks initiated from spherical defects as well as irregular-shaped lack of fusions. Closer inspection revealed that the cracks in a few of the Batch 1 specimens initiated from more than one defect grouped together as seen in **Fig. 7(a)**. Effectively, the closely grouped, smaller defects behaved as one big defect [9].

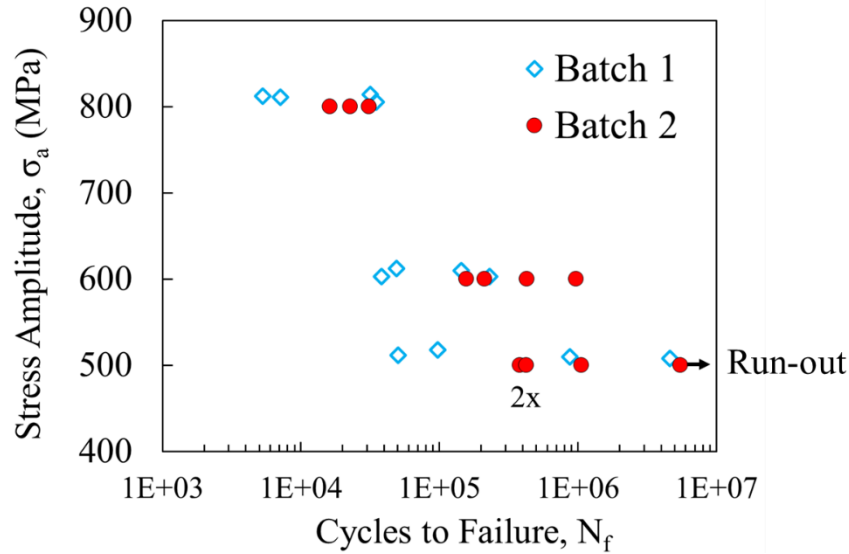


**Fig. 6** Stress-life fatigue behavior of L-PBF CA-H1025 17-4 PH SS machined specimens fabricated using Batch 1 and Batch 2 powder batches.

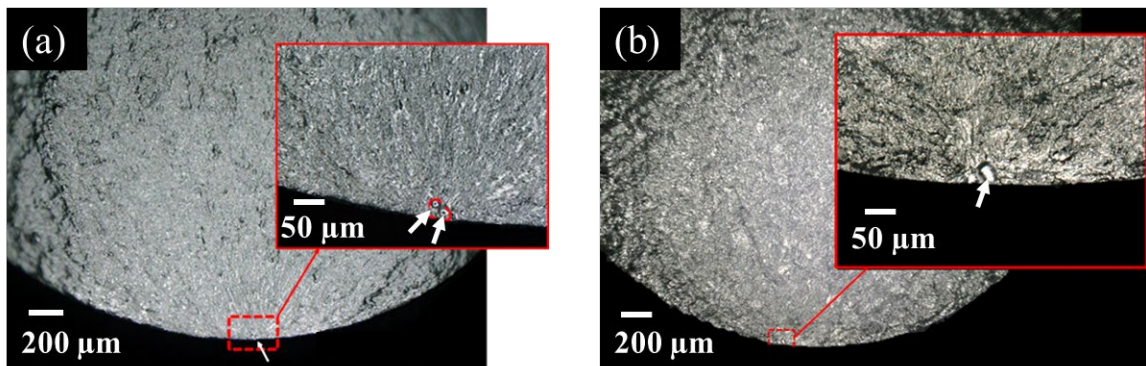


**Fig. 7** Fractography of L-PBF CA-H1025 17-4 PH SS machined specimens fabricated using (a) Batch 1 and (b) Batch 2.

### Conclusions

Characteristics of powder feedstocks such as particle morphology, particle size distribution, internal porosity, etc., were observed to influence their flowability, spreadability, packing state, etc. This resulted in different degrees of porosity in the fabricated specimens and thus, different fatigue performances. The conclusions drawn from this study are:

- The presence of finer powder particles and higher cohesive force between them resulted in the formation of agglomerates, and thus led to a poor packing state.
- Lower flowability and poor packing state of Batch 1 powder resulted in higher porosity in the fabricated specimens.
- Higher porosity deteriorated the fatigue resistance of Batch 1 specimens. In addition, it also resulted in more scatter in the fatigue lives of Batch 1 specimens as compared to Batch 2.
- Fatigue cracks were observed to initiate from spherical and irregular-shaped lack of fusion defects.

## Acknowledgments

This material is based upon the work partially supported by National Science Foundation (NSF) under grant # 1919818.

## References

- [1] W.E. Frazier, Metal additive manufacturing: A review, *J. Mater. Eng. Perform.* 23 (2014) 1917–1928. <https://doi.org/10.1007/s11665-014-0958-z>.
- [2] A. Cooke, J. Slotwinski, Properties of Metal Powders for Additive Manufacturing: A Review of the State of the Art of Metal Powder Property Testing, (n.d.). <https://doi.org/10.6028/NIST.IR.7873>.
- [3] R. Ghiaasiaan, A. Poudel, N. Ahmad, P.R. Gradl, S. Shao, N. Shamsaei, High Temperature Tensile and Fatigue Behaviors of Additively Manufactured IN625 and IN718, *Procedia Struct. Integr.* 38 (2022) 581–587. <https://doi.org/10.1016/J.PROSTR.2022.03.059>.
- [4] R. Ghiaasiaan, A. Poudel, N. Ahmad, M. Muhammad, P.R. Gradl, S. Shao, N. Shamsaei, Room Temperature Mechanical Properties of Additively Manufactured Ni-base Superalloys: A Comparative Study, *Procedia Struct. Integr.* 38 (2022) 109–115. <https://doi.org/10.1016/J.PROSTR.2022.03.012>.
- [5] M. Sakhakarmy, S. Tian, L. Raymond, G. Xiong, J. Chen, Y. Jin, Printability study of self-supporting graphene oxide-laponite nanocomposites for 3D printing applications, *Int. J. Adv. Manuf. Technol.* 114 (2021) 343–355. <https://doi.org/10.1007/S00170-021-06870-5/FIGURES/7>.
- [6] J.H. Tan, W.L.E. Wong, K.W. Dalgarno, An overview of powder granulometry on feedstock and part performance in the selective laser melting process, *Addit. Manuf.* 18 (2017) 228–255. <https://doi.org/10.1016/j.addma.2017.10.011>.
- [7] A. Mostafaei, C. Zhao, Y. He, S. Reza Ghiaasiaan, B. Shi, S. Shao, N. Shamsaei, Z. Wu, N. Kouraytem, T. Sun, J. Pauza, J. V. Gordon, B. Webler, N.D. Parab, M. Asherloo, Q. Guo, L. Chen, A.D. Rollett, Defects and anomalies in powder bed fusion metal additive manufacturing, *Curr. Opin. Solid State Mater. Sci.* 26 (2022) 100974. <https://doi.org/10.1016/J.COSSMS.2021.100974>.
- [8] N. Shamsaei, A. Yadollahi, L. Bian, S.M. Thompson, An overview of Direct Laser Deposition for additive manufacturing; Part II: Mechanical behavior, process parameter optimization and control, *Addit. Manuf.* 8 (2015) 12–35. <https://doi.org/10.1016/j.addma.2015.07.002>.
- [9] A. Soltani-Tehrani, J. Pegues, N. Shamsaei, Fatigue behavior of additively manufactured 17-4 PH stainless steel: The effects of part location and powder re-use, *Addit. Manuf.* 36 (2020) 101398. <https://doi.org/10.1016/j.addma.2020.101398>.
- [10] P.D. Nezhadfar, A. Soltani-Tehrani, A. Sterling, N. Tsolas, N. Shamsaei, P. Dastranjy Nezhadfar, A. Soltani-Tehrani, A. Sterling, N. Tsolas, N. Shamsaei, The effects of powder recycling on the mechanical properties of additively manufactured 17-4 PH stainless steel, *Proc. 29th Annu. Int. Solid Free. Fabr. Symp. – An Addit. Manuf. Conf.* (2018) 1292–1300.
- [11] P.E. Carrion, A. Soltani-Tehrani, N. Phan, N. Shamsaei, Powder Recycling Effects on the Tensile and Fatigue Behavior of Additively Manufactured Ti-6Al-4V Parts, *J. Miner. Met. Mater.* 71 (2019) 963–973. <https://doi.org/10.1007/s11837-018-3248-7>.
- [12] A. Soltani-Tehrani, M. Habibnejad-Korayem, S. Shao, M. Haghshenas, N. Shamsaei, Ti-6Al-4V powder characteristics in laser powder bed fusion: The effect on tensile and fatigue

- behavior, *Addit. Manuf.* 51 (2022) 102584. <https://doi.org/10.1016/J.ADDMA.2021.102584>.
- [13] A. Poudel, N. Shamsaei, S. Shao, Linear elastic finite element calculations of short cracks initiated from the defects : effect of defect shape and size, 2021 *Int. Solid Free. Fabr. Symp.* (2021) 915–922.
- [14] A. Poudel, A. Soltani-Tehrani, S. Shao, N. Shamsaei, Effect of powder characteristics on tensile properties of additively manufactured 17-4 PH stainless steel, 2021 *Int. Solid Free. Fabr. Symp.* (2021).
- [15] Lerma, A Comprehensive Approach to Powder Feedstock Characterization for Powder Bed Fusion Additive Manufacturing A Case Study on AlSi7Mg, (2018).
- [16] A. Simchi, The role of particle size on the laser sintering of iron powder, *Metall. Mater. Trans. B Process Metall. Mater. Process. Sci.* 35 (2004) 937–948. <https://doi.org/10.1007/s11663-004-0088-3>.
- [17] A. Soltani-Tehrani, J. Pegues, N. Shamsaei, Powder recycling of 17-4 PH SS, *Addit. Manuf.* (2020).
- [18] A. Strondl, O. Lyckfeldt, H. Brodin, U. Ackelid, Characterization and Control of Powder Properties for Additive Manufacturing, 431 (n.d.) 37. <https://doi.org/10.1007/s11837-015-1304-0>.
- [19] America Makes, AMSC, Standardization Roadmap for Additive Manufacturing, 2018.
- [20] I. Mutlu, E. Oktay, Characterization of 17-4 PH stainless steel foam for biomedical applications in simulated body fluid and artificial saliva environments, *Mater. Sci. Eng. C.* 33 (2013) 1125–1131. <https://doi.org/10.1016/J.MSEC.2012.12.004>.
- [21] S.S.M. Tavares, J.S. Corte, J.M. Pardal, Failure of 17-4 PH stainless steel components in offshore platforms, *Handb. Mater. Fail. Anal. with Case Stud. from Oil Gas Ind.* (2016) 353–370. <https://doi.org/10.1016/B978-0-08-100117-2.00019-4>.
- [22] P.D. Nezhadfar, R. Shrestha, N. Phan, N. Shamsaei, Fatigue behavior of additively manufactured 17-4 PH stainless steel: Synergistic effects of surface roughness and heat treatment, *Int. J. Fatigue.* 124 (2019) 188–204. <https://doi.org/10.1016/j.ijfatigue.2019.02.039>.
- [23] ASTM E466-15, Standard Practice for Conducting Force Controlled Constant Amplitude Axial Fatigue Tests of Metallic Materials, 03 (2002) 4–8.
- [24] American Society for Testing Material, Standard test method for shear testing of powders using the freeman technology FT4 powder rheometer shear cell, *Astm D7891-15.* (2015) 1–11. <https://doi.org/10.1520/D7891-15.1.5>.
- [25] T. Allen, Particle Size Measurement, Springer Netherlands, Dordrecht, 1990. <https://doi.org/10.1007/978-94-009-0417-0>.
- [26] Object Research Systems (ORS) Inc, Dragonfly, (2021). <http://www.theobjects.com/dragonfly>.
- [27] C.A. Schneider, W.S. Rasband, K.W. Eliceiri, NIH Image to ImageJ: 25 years of image analysis, *Nat. Methods* 2012 97. 9 (2012) 671–675. <https://doi.org/10.1038/nmeth.2089>.
- [28] W. Wle, An overview of powder granulometry on feedstock and part performance in the selective laser melting process, (2017). <https://doi.org/10.1016/j.addma.2017.10.011>.
- [29] S.E. Brika, M. Letenneur, C.A. Dion, V. Brailovski, Influence of particle morphology and size distribution on the powder flowability and laser powder bed fusion manufacturability of Ti-6Al-4V alloy, *Addit. Manuf.* 31 (2020) 100929. <https://doi.org/10.1016/j.addma.2019.100929>.

- [30] A.A. Martin, N.P. Calta, S.A. Khairallah, J. Wang, P.J. Depond, A.Y. Fong, V. Thampy, G.M. Guss, A.M. Kiss, K.H. Stone, C.J. Tassone, J. Nelson Weker, M.F. Toney, T. van Buuren, M.J. Matthews, Dynamics of pore formation during laser powder bed fusion additive manufacturing, *Nat. Commun.* 10 (2019) 1–10. <https://doi.org/10.1038/s41467-019-10009-2>.
- [31] A.T. Sutton, C.S. Kriewall, M.C. Leu, J.W. Newkirk, Powder characterisation techniques and effects of powder characteristics on part properties in powder-bed fusion processes, *Virtual Phys. Prototyp.* 12 (2017) 3–29. <https://doi.org/10.1080/17452759.2016.1250605>.
- [32] M. Iebba, A. Astarita, D. Mistretta, I. Colonna, M. Liberini, F. Scherillo, C. Pirozzi, R. Borrelli, S. Franchitti, A. Squillace, Influence of Powder Characteristics on Formation of Porosity in Additive Manufacturing of Ti-6Al-4V Components, *J. Mater. Eng. Perform.* 26 (2017) 4138–4147. <https://doi.org/10.1007/s11665-017-2796-2>.
- [33] S.M.H. Hojjatzadeh, N.D. Parab, Q. Guo, M. Qu, L. Xiong, C. Zhao, L.I. Escano, K. Fezzaa, W. Everhart, T. Sun, L. Chen, Direct observation of pore formation mechanisms during LPBF additive manufacturing process and high energy density laser welding, *Int. J. Mach. Tools Manuf.* 153 (2020) 103555. <https://doi.org/10.1016/j.ijmachtools.2020.103555>.